

See discussions, stats, and author profiles for this publication at: <https://www.researchgate.net/publication/312131517>

# Etching-Controlled Growth of Graphene by Chemical Vapor Deposition

Article in *Chemistry of Materials* · January 2017

DOI: 10.1021/acs.chemmater.6b03672

---

CITATIONS

11

READS

148

6 authors, including:



Birong Luo

University of Cambridge

27 PUBLICATIONS 453 CITATIONS

[SEE PROFILE](#)



Enlai Gao

Wuhan University

39 PUBLICATIONS 269 CITATIONS

[SEE PROFILE](#)



Dechao Geng

National University of Singapore

59 PUBLICATIONS 1,469 CITATIONS

[SEE PROFILE](#)



Wang Huaping

Chinese Academy of Sciences

15 PUBLICATIONS 139 CITATIONS

[SEE PROFILE](#)

Some of the authors of this publication are also working on these related projects:



Microstructural Evolution and Life Prediction of Materials [View project](#)



Microscale Mechanisms of Energy Dissipation [View project](#)

# Etching-Controlled Growth of Graphene by Chemical Vapor Deposition

Birong Luo,<sup>†</sup> Enlai Gao,<sup>‡,ID</sup> Dechao Geng,<sup>†</sup> Huaping Wang,<sup>†</sup> Zhiping Xu,<sup>\*,‡</sup> and Gui Yu<sup>\*,†,§,ID</sup>

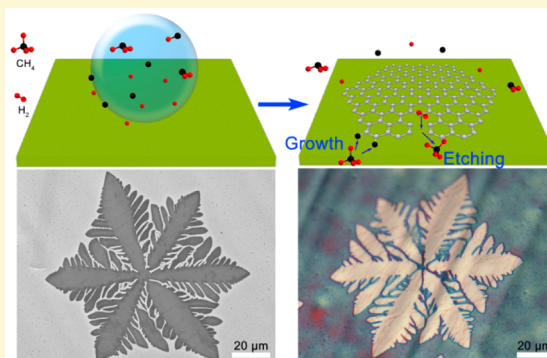
<sup>†</sup>Beijing National Laboratory for Molecular Sciences, Institute of Chemistry, Chinese Academy of Sciences, Beijing 100190, P. R. China

<sup>‡</sup>Applied Mechanics Laboratory, Department of Engineering Mechanics, and Center for Nano and Micro Mechanics, Tsinghua University, Beijing 100084, P. R. China

<sup>§</sup>University of Chinese Academy of Sciences, Beijing 100049, China

## Supporting Information

**ABSTRACT:** Graphene growth and etching are reciprocal processes that can reach a dynamic balance during chemical vapor deposition (CVD). Most commonly, the growth of graphene is the dominate process, while the etching of graphene is a recessive process often neglected during CVD growth of graphene. We show here that through the rational design of low-pressure CVD of graphene in hydrogen-diluted methane and regulation of the flow rate of H<sub>2</sub>, the etching effect during the growth process of graphene could be prominent and even shows macroscopic selectivity. On this basis, etching-controlled growth and synthesis of graphene with various morphologies from compact to dendritic even to fragmentary have been demonstrated. The morphology-selection mechanism is clarified through phase-field theory based on simulations. This study not only presents an intriguing case for the fundamental mechanism of CVD growth but also provides a facile method for the synthesis of high-quality graphene with trimmed morphologies.



## INTRODUCTION

Graphene grown on copper by chemical vapor deposition (CVD) has been significantly explored for the synthesis of high-quality graphene since the popular recipe for single-layer graphene growth was introduced in 2009,<sup>1</sup> many years after the first report of the deposition of graphene on Cu in 1992.<sup>2</sup> Intensive effort has been spent to develop strategies for growing high-quality graphene with controlled size, morphology, edge structures, and layer numbers<sup>3–9</sup> and to further extend this growth to improve our understanding of the growth mechanism. At the same time, graphene etching has always been a hot spot of graphene research. Many studies of graphene etching have shown the etching behavior and kinetics using different etchants such as hydrogen, air, and metal nanoparticles.<sup>10–13</sup> Although extensive studies have been conducted to explore the behaviors and mechanism of CVD growth<sup>14</sup> or etching of graphene,<sup>10,11</sup> some of the processes involved during CVD remain unresolved. For instance, little is known about the factors that balance growth and etching kinetics during the same CVD process and then control graphene morphology and edge structure. Indeed, the occurrence of both hexagonally shaped and dendritic flakes is a common phenomenon that remains to be elucidated. Therefore, it is highly desirable to clarify the dynamic processes and corresponding dependence between growth and etching in the same CVD process where graphene growth is always accompanied by its etching. These

two parts are competitive and strongly dependent on each other during the CVD process.<sup>15–17</sup>

On the other hand, to improve our understanding of the CVD graphene mechanism and to better control the growth of high-quality graphene, it is crucial to understand how growth and etching kinetics interact and then affect defect formation during CVD growth of graphene. It is necessary to note that this effort is complicated in the case of a hydrogen-diluted carbon source for growth, because the hydrogen contribution seems to serve a double role. As an activator of surface-bound carbon, hydrogen leads to graphene growth. Meanwhile, hydrogen also induces etching of graphene as an etching reagent to control the size and morphology of the resulting graphene.<sup>15</sup> For a long time, certain aspects of the role of hydrogen, in particular, the hydrogen-induced etching effects during the CVD growth of graphene, remain unclear, and the hope is that a systematic investigation could disinter all of the graphene patterns.

Here, we focus on analysis of the detailed effects of etching based on growth and then the control over the morphology and structure of graphene during low-pressure CVD on copper. By adjusting the growth parameters, we could modulate the related

Received: August 31, 2016

Revised: January 5, 2017

Published: January 6, 2017

extent between growth and etching and then find the CVD growth window, in which graphene growth and etching are strongly dependent on the controls of the unique morphology and structured modalities of the resulting graphene. In our experiments, via regulation of the flow rates of hydrogen, a series of graphene patterns from compact to dendritic morphology and ultimately to graphene fragments were obtained. These unique graphene patterns show an apparent etching trace, providing direct evidence of the etching-controlled growth of graphene.

## ■ EXPERIMENTAL SECTION

**Material.** Cu foil (99.8% pure, 25  $\mu\text{m}$  thick) was obtained from Alfa Aesar (Tianjin, China).

**CVD Synthesis and Transfer of Graphene.** Cu foils were loaded into a 1 in. quartz CVD tube mounted inside a furnace (Lindberg/Blue M, TF5503SA, Thermo Fisher Scientific Inc., Asheville, NC). The system was pumped from ambient pressure to  $\sim 3$  Pa to clean the whole system and then filled with a 200 sccm (standard cubic centimeters per minute)  $\text{H}_2$  gas flow. Subsequently, the Cu foils were heated (30–40 min) and annealed at 1020 °C in a pure  $\text{H}_2$  gas for 30 min at ambient pressure. At the beginning of growth, the  $\text{H}_2$  flow rates were adjusted to the desired values, and the needle valve to the pump was opened. As soon as the pressure stabilized,  $\text{CH}_4$  was then introduced into the chamber for low-pressure CVD growth of graphene (the growth pressures are listed in Table S1). After growth for a certain period of time, the  $\text{CH}_4$  flow was turned off, and the system was cooled to room temperature by simply opening the furnace.

A commonly used method of bubbling combined with poly(methyl methacrylate) was employed to transfer graphene from Cu surfaces onto 300 nm  $\text{SiO}_2/\text{Si}$  substrates and TEM (transmission electron microscopy) grids. The poly(methyl methacrylate)-supported films were finally dissolved with hot acetone.

**Characterization of Graphene.** Scanning electron microscopy (SEM) (Hitachi S-4800, 1 kV, Hitachi, Ltd., Tokyo, Japan) and optical microscopy were used to observe the morphology of as-produced graphene before and after transfer. Raman spectroscopy and Raman mapping (Renishaw inVia Plus, with laser excitation at 514 nm and a spot size of 1–2  $\mu\text{m}$ , Renishaw plc, Gloucestershire, U.K.) were performed throughout the graphene transferred onto 300 nm  $\text{SiO}_2/\text{Si}$  substrates to characterize the quality and homogeneity. TEM (Tecnai G2 F20 U-TWIN, operated at 200 kV, FEI, Hillsboro, OR) combined with SAED (selected area electron diffraction) was used to characterize the crystallinity of as-grown graphene.

## ■ RESULTS AND DISCUSSION

As shown in Figure 1a, we designed and conducted the low-pressure CVD experiments in which pure hydrogen gas was employed to dilute methane for graphene growth. It is found that the role of hydrogen is dual, which acts as an activator to favor the growth of graphene and as a highly selective etchant to trim the graphene crystals. Panels b and c of Figure 1 show typical results in magnified SEM images; star-shaped graphene was formed with a strong etching effect and distributed well on a Cu surface at 1020 °C using 0.5 sccm  $\text{CH}_4$  and 20 sccm  $\text{H}_2$  during growth for  $\sim 30$  min. Interestingly, these graphene crystals were trimmed into large amounts of graphene debris, which were dispersed well in a star-shaped profile (Figure 1c).

Considering that pure hydrogen gas was employed as the only carrier gas in our experiment, the etching was largely attributed to the hydrogen that partly acts as a highly selective etchant to sculpt the graphene crystals<sup>15</sup> as mentioned above. Therefore, we manipulated the  $\text{CH}_4/\text{H}_2$  flow rate ratio to explore the detailed etching effects and then control the growth of the resulting graphene. Figure 2a–h shows a series of SEM

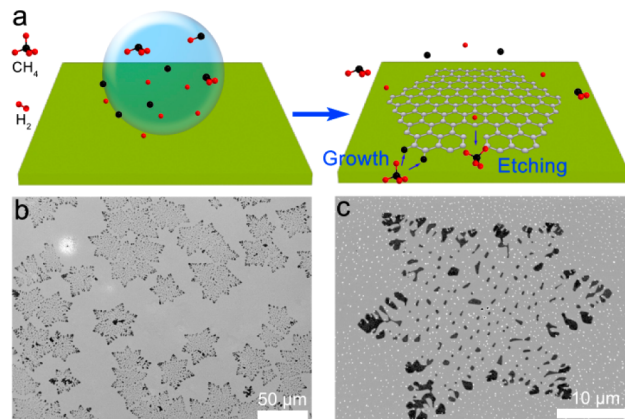


**Figure 1.** Etching-controlled growth of graphene fragments on a Cu surface. (a) Schematic illustration showing the process of etching-controlled growth during CVD of graphene in  $\text{H}_2$ -diluted  $\text{CH}_4$ . (b) SEM image of the well-dispersed graphene fragments produced on a Cu surface using 0.5 sccm  $\text{CH}_4$  and 20 sccm  $\text{H}_2$  for  $\sim 30$  min. (c) Magnified SEM image of an individual graphene fragment.

images of typical graphene with etching-controlled growth on Cu surfaces at different  $\text{H}_2$  flow rates (15, 20, 25, 30, 35, 40, 45, and 50 sccm, respectively) listed in Table S1. During graphene growth, we changed the flow rate of  $\text{H}_2$  only from batch to batch at the fixed flow rate of  $\text{CH}_4$  (0.5 sccm). As shown in Figure 2a–h, the morphology of the as-grown graphene transforms in a definite way from fragmental to compact with the increase of  $\text{H}_2$  flow rate. This apparently indicates that the role of hydrogen is significant for the formation of this particularly special graphene under such CVD conditions. It is believed that the hydrogen could etch the as-grown graphene away during the growth process. Also, our observation partly corresponds to some phenomena observed in previous studies.<sup>3,9,18–20</sup> However, most of these studies mainly focused on the growth behavior to consider this phenomenon without regard for the etching effects. Actually, etching would happen during CVD growth when the  $\text{CH}_4/\text{H}_2$  flow rate ratio was being modulated.<sup>21,22</sup> Here, our results demonstrate that the etching did happen and could be employed to control the growth of graphene, especially for the control over their morphologies and structures. The etching effects can be confirmed from panels a and b of Figure S1. As shown, a typical high-magnification SEM image (Figure S1a, taken from the rectangular area in Figure S1b) unequivocally shows a hexagonal hole and 120° V-shaped gaps induced by etching, consistent with the previous anisotropic hydrogen etching results,<sup>23</sup> indicating the etching nature during the growth. In addition, these graphenes with etching-controlled growth appeared to align over a large area and showed high reproducibilities and high yields (Figure 3a and Figure S2).

To further evaluate the quality and uniformity of the graphene, we transferred it onto  $\text{SiO}_2/\text{Si}$  substrates and characterized it through Raman spectra. As shown in panels b and c of Figure 3, optical images before and after the transfer show the apparent contrast of the etched trace with respect to the substrates. Figure 3d exhibits typical Raman spectra taken randomly from Figure 3c. We learned that the graphene displays typical single-layer features with two prominent Raman peaks located at  $\sim 1580$  and  $\sim 2680 \text{ cm}^{-1}$ , corresponding to the G and 2D peaks, respectively. Micro-Raman spatial mapping also was used to further investigate the uniformity of as-grown

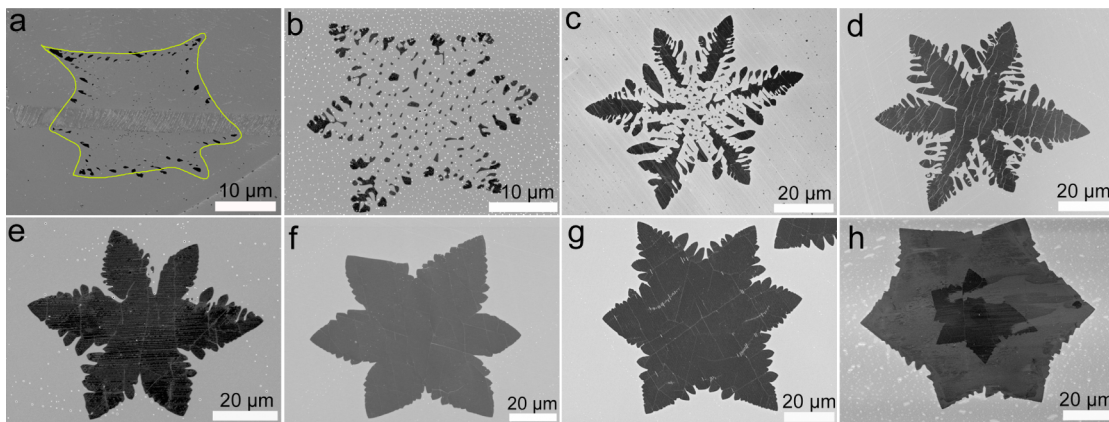


**Figure 2.** Magnified SEM images of graphene with etching-controlled growth using 0.5 sccm CH<sub>4</sub> and varied H<sub>2</sub> flow rates [(a–h) 15, 20, 25, 30, 35, 40, 45, and 50 sccm, respectively] as summarized in Table S1. The growth time was set to ~30 min.

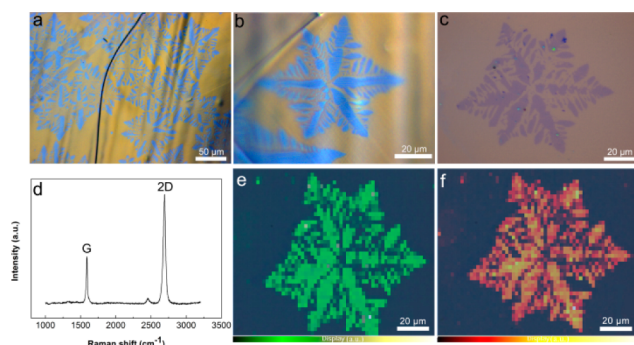


**Figure 3.** Optical characterizations and Raman spectra of graphene with etching-controlled growth using 0.5 sccm CH<sub>4</sub> and 25 sccm H<sub>2</sub> for ~30 min. (a) Optical image showing dendritic graphene flakes with etching-controlled growth distributed on a Cu surface. (b and c) Magnified optical images of as-grown graphene before and after the transfer to the SiO<sub>2</sub>/Si substrate, respectively. (d) Typical Raman spectrum measured from panel c. (e and f) Intensity mapping of the 2D and G Raman peaks of panel c.

graphene. As shown in panels e and f of Figure 3, the intensity mapping of characterized peaks of 2D and G shows the high uniformity with an inconsistent color distribution corresponding to the etched trace across the whole graphene crystal. This observation agrees well with the optical image.

In addition, TEM and SAED were performed to determine the crystalline structure of the graphene with etching-controlled growth. Prior to TEM observation, transferred graphene samples were located by SEM. Panels a and b of Figure 4 show low- and high-magnification SEM images of the graphene transferred onto a holey carbon-supported TEM grid. The brighter contrast of graphene on holey supporting films is evidence of the dendritic morphology, indicating the successful transfer of graphene. Because the whole graphene domain is difficult to identify in a normal bright-field TEM view field, a single lobe of the graphene was taken according to the SEM image for the TEM characterization (Figure 4c). As shown, a graphene membrane spanning the hole of the carbon film can be clearly seen in the TEM image in Figure 4c. Then extensive SAED patterns were acquired from different regions marked with red, pink, yellow, and blue colors in Figure 4c. As shown, Figure 4d–g corresponds to different regions generated by a single set of hexagon diffraction pattern characteristics. More importantly, no rotation angle between different regions was

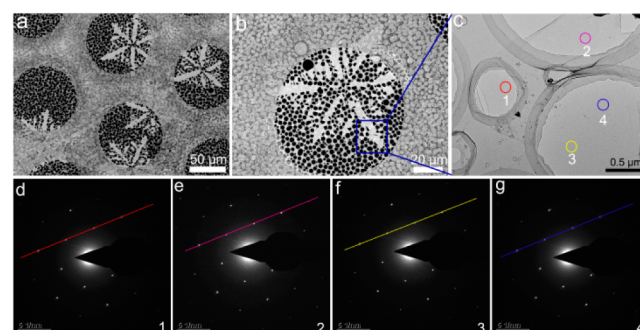


**Figure 4.** TEM characterizations of graphene with etching-controlled growth (0.5 sccm CH<sub>4</sub> and 25 sccm H<sub>2</sub> for ~30 min). (a and b) Low- and high-magnification SEM images, respectively, of dendritic graphene with etching-controlled growth after the transfer onto a holey carbon-supported TEM grid. (c) TEM image of a graphene lobe taken from panel b. (d–g) Representative SAED patterns corresponding to the regions marked by different numbers in panel c.

observed as shown in Figure 4d–g, revealing that the graphene domain has a single-crystalline nature. In other words, both the growth and etching act on the same graphene crystal and result in unique morphology and edge modalities.

On the basis of the results presented above, some preliminary points of the etching-controlled growth of graphene can be confirmed. First, with the increase of H<sub>2</sub> flow rates (or partial pressure P<sub>H<sub>2</sub></sub>), it seems that growth would increasingly dominate the CVD process, producing more and more compact graphene. This can be confirmed from Figure 2a–h. Second, the hydrogen-induced etching of graphene definitely happened simultaneously during the CVD growth of graphene, and both the growth and the etching were strongly dependent on each other in controlling the morphology and structure of graphene. Third, hydrogen plays a critical role in determining the competition between growth and etching of graphene based on the low-pressure CVD conditions. It is reported that H<sub>2</sub> acts as a catalyst to promote the activation of adsorbed methane toward hydrocarbon radicals and activate the Cu surface for bonding the active C atoms.<sup>15,20</sup> On the other hand, the H<sub>2</sub> also functions as a decomposition inhibitor of methane or an etchant of graphene based on the equilibrium reaction between methane and hydrogen. Therefore, here we qualitatively divide the CVD process into two parts (growth and etching) as diagrammatically shown in Figure 5a. With an

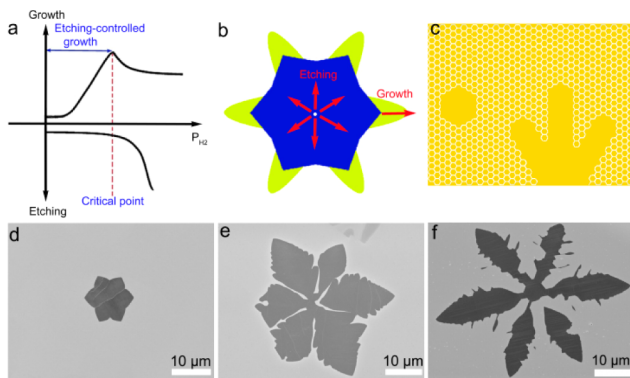


**Figure 5.** Etching-controlled growth mechanism of CVD graphene and its evolution with time. (a) Diagrammatic illustration showing the process of etching and growth as a function of hydrogen partial pressure. (b) Schematic illustration of a compact (blue) island evolving into a six-lobed shape (yellow) during etching-controlled growth. (c) Schematic diagram of the hydrogen etching mode. (d–f) Evolution of etching-controlled growth of an individual graphene island recorded as a function of time at 5, 20, and 30 min, respectively, with CVD conditions of 0.5 sccm  $\text{CH}_4$  and 30 sccm  $\text{H}_2$  at 1020 °C.

increasing  $\text{H}_2$  flow rate (that can be qualified by  $P_{\text{H}_2}$ ), the contribution of growth to the change in graphene morphology would increase sharply first and then reach a balanced level. Meanwhile, the contribution of etching would always be smaller than that of growth and increases very slowly until it reaches a critical point. At this critical point and even in some range near this critical point, we found that the resulting changes in graphene morphologies could not be discerned, mostly showing rough edges. However, a normal hexagonal shape of graphene should also be grown by regulating the partial pressure of hydrogen according to the method described in ref 15. Simply, it is not easy to find the exact windows for the growth of the normal hexagonal shape of graphene under such a wide  $P_{\text{H}_2}$  range. Indeed, in our experiments, if we increased the  $\text{H}_2$  flow rate beyond this critical value to a quite high value, the total effect (growth + etching) for graphene synthesis would be suppressed largely just because of the strong etching and its decomposition inhibition of methane based on the equilibrium reaction. In general terms, the moderate amount of  $\text{H}_2$  was preferred for the growth of graphene, and the etching effects would be covered by growth. Therefore, there were not obvious etching effects observed in the relatively high  $P_{\text{H}_2}$  range, which is dominated by the rate-limited growth process. During this rate-limited process, the growth of graphene is more favorable because of the adequate catalysis of hydrogen to promote the activation of adsorbed methane and activate the Cu surface, which is more likely to allow the transport of carbon species through the Cu surface to the graphene edge and expand the graphene layer. This process gives priority to the growth rate and then leads to faster and more compact growth of graphene with an increased  $P_{\text{H}_2}$  (Figure 2a–h). To make the etching effects prominent, we chose a quite low methane flow rate (0.5 sccm) for growth. On this basis, when the amount of  $\text{H}_2$  is decreased below the critical point, the etching will emerge gradually and then control the growth of graphene, which indeed marks a striking way to frame diverse morphologies of graphene as demonstrated above. It is necessary to point out that although the etching ability of hydrogen is poor at relatively low flow rates, this can nonetheless result in strong

etching effects, as its capacity to etch will always be present and constant while its effects on growth are decreased sharply.

Then, what effect does etching have on the growth of graphene for shaping the special graphene morphology in this very complicated growth and etching system? First, we found that the growth of graphene always tends to produce a starlike shape rather than a perfect hexagon when  $P_{\text{H}_2}$  is being reduced, which was attributed to a transition from a rate-limited to diffusion-limited growth regime.<sup>24,25</sup> This mostly resulted from the role of hydrogen here. It illustrates that the concentration gradient of the active carbon source is greater at the corners, where the graphene crystal grows faster, resulting in a starlike shape. Under the guidance of this general picture, we could analyze the etching system in a simplified manner and provide possible explanations for detailed observations in our etching-controlled growth of graphene.

The etching process is the reverse of graphene growth, as hydrogen can react with carbon in graphene with the catalytic function of the copper substrate underneath and produce methane. Like nucleation during growth, nuclei of etching graphene would form in the initial stage of etching. As Figure 5b shows, during the growth of graphene, the etching nuclei preferentially exist near the nucleation site for growth where the lowest reaction barrier would make it easier to proceed, leading to etching openings. On the basis of these etching openings, the etched area would expand and form etching channels with the continued supply and diffusion of hydrogen molecules on graphene. It should be noted that the etching channels include but are not limited to a straight etching channel. As schematically shown in Figure 5c, the etching front could branch out and change direction mainly because of the fluctuation of hydrogen molecule diffusion along the etched edge of graphene, leading to a fractal etching mode.<sup>11</sup> Interestingly, the sharp turns were found to be highly uniform, largely at 30° and 120° under our experimental conditions, indicating an etching direction and/or edge preference.<sup>26</sup> According to ref 10, this preference of crystallographic orientations of etching in graphene tends to be in a zigzag direction with 120° anisotropic hydrogen etching. However, we note that the etching sharp turns formed here also include 30°. With this uniformity in the etching angles between them, both triangularly and hexagonally shaped graphene debris (Figure S3a) could be formed after the etching process ends. After looking closely in some smaller areas, we can find a uniform triangularly (Figure S3b) or hexagonally (Figure S3c) shaped graphene array of debris. It should be noted the triangular graphene pieces formed here result from 30° sharp turns and consist of edges with different (zigzag or arm chair) crystallographic orientations. This can be distinguished from Figure 5c. The suggested zigzag and arm chair edges are also shown in Figure S3b for the sake of clarity. In addition, we also observed the etched hexagon hole (Figure S1) during the etching-controlled growth process. It is suggested that particles on graphene are largely responsible for this hexagon hole etching,<sup>23</sup> and the etching reaction is initiated by hydrogenation in locations where they were deposited.

To fully understand this coexistence of etching during CVD graphene growth, a further experiment with a different growth time was performed for comparison. Figure 5d–f shows the etching-controlled growth behavior of individual graphene flakes as a function of time. The clear indication is that growth dominated the CVD process in the first 5 min and showed the

starlike shape due to diffusion-limited growth (Figure 5d). Then the etching would emerge on the basis of the growth and start from the nucleation center of graphene to form the dominant etching pathways (Figure 5e). It is important to note here that it takes time to initialize the nuclei for etching at the beginning of graphene growth. Therefore, in the first 5 min, graphene growth dominates over etching. As the growth time further increased, the resulting graphene was gradually etched away, forming the branched graphene pattern (Figure 5f). During this whole evolution, we find that the dominance of growth and/or etching would partly depend on the size of graphene, but as soon as the etching takes into account the growth process and comes to a stable state, the ultimate dominance between growth and etching would comply with the hypothesis depicted in Figure 5a. It is also important to point out that the growth is always occurring during the CVD process, but at the same time, the rate of flux of carbon into these narrow etched channels is low. This would yield more complicated growth processes by refilling growth following the etched area, and by edge attachment, diffusion, and growth along the edges, forcing the graphene profile to change throughout the whole process.  $P_{H_2}$  governs the competitive kinetics between growth and etching, and the etching/growth contribution ratio, finally leading to rich and widely varying graphene patterns.

To verify the mechanism of growth–etching competition proposed in Figure 5a and the formation of an etching-controlled growth pattern, we constructed a phase-field model as detailed in the methods section in the *Supporting Information*. In this model, we include the growth, etching of graphene crystals, and diffusion of carbon species on the substrate. Additionally, considering the graphene growth on Cu begins with an influx of precursors onto the Cu surface, the rate of flux of precursors ( $F$ ) onto the Cu surface and further the concentration of the carbon species ( $u$ ) would play an important role in controlling the growth dynamics. In fact, we indeed find that deposition flux  $F$  and equilibrium carbon concentration  $u_{eq}$  on the substrate critically control the competition between growth and etching processes. By changing these parameters, we can successfully produce the graphene patterns to a largest extent (see Figure S4). Figure S4 clearly shows how  $F$  and  $u_{eq}$  impact growth and etching then with respect to the formation of varied graphene patterns. The amplitude of  $F$ , compared to the diffusion constant  $D$  ( $F/D$ ), determines whether the growth is limited by diffusion or reaction rate. The relation between a local concentration  $u$  and  $u_{eq}$  determines whether the growth ( $u > u_{eq}$ ) or etching ( $u < u_{eq}$ ) process is dominant. As  $F$  decreases from bottom to top and  $u_{eq}$  increases from left to right, the simulated growth behavior features a growth transition from rate-limited growth (compact patterns in the bottom left area) to diffusion-limited growth with etching controlled (dendritic patterns in the top right area), which exactly corresponds to our experimental observations. That is what we experimentally observed above: by regulating the  $H_2$  flow rate ( $P_{H_2}$ ), we can modulate the competition between growth and etching and then transform the resulting graphene patterns from compact to dendritic morphology. More importantly, it is true that the values of  $F$  and  $u_{eq}$  both depend on  $P_{H_2}$  that we used as the key tuning parameter in experiments; in other words,  $F/u_{eq}$  increases (decreases) with  $P_{H_2}$  (decrease) at the low-pressure limit. On this basis, we draw a two-way arrow indicating  $H_2$  changes as

depicted in Figure S4, which clearly indicate that with an increase or decrease in the  $H_2$  flow rate ( $P_{H_2}$ ), the  $F/u_{eq}$  ratio increases or decreases, respectively, and the dominance of etching is weakened or enhanced, respectively. In addition, by matching  $F$  and  $u_{eq}$  properly according to our experimental conditions, we successfully reproduce the graphene patterns characterized experimentally (Figure 6). These simulation results, with unambiguous physics embedded, further validate our explanation based on the growth–etching balance.

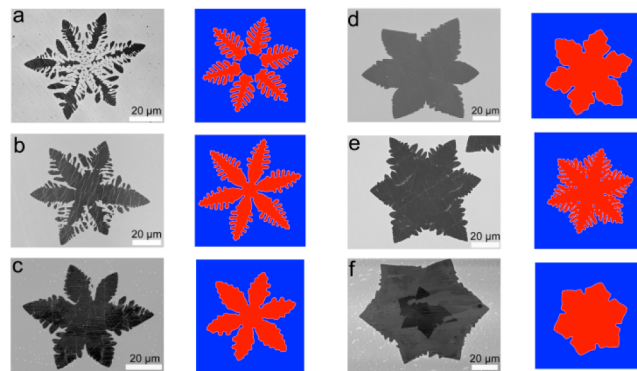


**Figure 6.** Morphologies of CVD-grown graphene that resulted from the competition between growth and etching processes. The samples obtained from experiments (gray SEM images) match well simulated patterns from phase-field model predictions (red). The  $H_2$  flow rates in experiments were 25, 30, 35, 40, 45, and 50 sccm in panels a–f, respectively, with 0.5 sccm  $CH_4$ . The  $F$  and  $u_{eq}$  values are 0.004 and 0.04, 0.002 and 0.04, 0.001 and 0.02, 0.001 and 0.008, 0.008 and 0.02, and 0.004 and 0.004, respectively [dimensionless (see the *Supporting Information* for details)].

The results described above clearly suggest that a competitive etching process exists along with the growth process during the formation of graphene. Nevertheless, as we have demonstrated, the approach is based on a quite low flow rate of  $CH_4$  (0.5 sccm) to make the etching effects more prominent. If we increase the  $CH_4$  concentration, the graphene growth part would take over the whole CVD process and high-quality monolayer graphene sheets and even bilayer graphene could be obtained. As shown in Figure S5, when the flow rate of  $CH_4$  was increased from 0.5 to 5 sccm, it is conceivable that such etching effects become increasingly obscure and result in the formation of conventional graphene.

## ■ CONCLUSION

In conclusion, we have systematically studied the etching effects during the CVD growth of graphene by regulating the growth parameters mainly related to hydrogen and demonstrated that hydrogen plays a dual role in the CVD process. The hydrogen-induced etching and growth of graphene are strongly dependent on each other in controlling the formation of graphene morphology, which results in the morphological evolution of graphene patterns from fragmentary to branched to compact. In addition, a phase-field model was constructed to further confirm the etching-controlled growth of graphene and successfully reproduced the graphene patterns characterized experimentally. This discovery represents an unrevealed intrinsic etching-controlled growth of graphene and provides insight into the growth and etching mechanism of CVD graphene, which may apply to a wide range of other two-dimensional materials. More importantly, this method could

provide a simple but efficient method for controllably trimming graphene toward the construction of modality-tunable graphene gadgets, which are anticipated to possess unique properties and show potential in applications such as electronic devices.

## ■ ASSOCIATED CONTENT

### S Supporting Information

The Supporting Information is available free of charge on the ACS Publications website at DOI: [10.1021/acs.chemmater.6b03672](https://doi.org/10.1021/acs.chemmater.6b03672).

Additional images, spectra, and theoretical simulation methods ([PDF](#))

## ■ AUTHOR INFORMATION

### Corresponding Authors

\*E-mail: [yugui@iccas.ac.cn](mailto:yugui@iccas.ac.cn).

\*E-mail: [xuzp@tsinghua.edu.cn](mailto:xuzp@tsinghua.edu.cn).

### ORCID

Enlai Gao: [0000-0003-1960-0260](https://orcid.org/0000-0003-1960-0260)

Gui Yu: [0000-0001-8324-397X](https://orcid.org/0000-0001-8324-397X)

### Notes

The authors declare no competing financial interest.

## ■ ACKNOWLEDGMENTS

This work was supported by the National Natural Science Foundation of China (61390502), the National Major State Basic Research Development Program (2013CB933403), and the Strategic Priority Research Program of the Chinese Academy of Sciences (XDB 12030100).

## ■ REFERENCES

- (1) Li, X.; Cai, W.; An, J.; Kim, S.; Nah, J.; Yang, D.; Piner, R.; Velamakanni, A.; Jung, I.; Tutuc, E.; Banerjee, S. K.; Colombo, L.; Ruoff, R. S. Large-Area Synthesis of High-Quality and Uniform Graphene Films on Copper Foils. *Science* **2009**, *324*, 1312–1314.
- (2) Alstrup, I.; Chorkendorff, I.; Ullmann, S. The Interaction of CH<sub>4</sub> at High Temperatures with Clean and Oxygen Precovered Cu(100). *Surf. Sci.* **1992**, *264*, 95–102.
- (3) Li, X.; Magnuson, C. W.; Venugopal, A.; Tromp, R. M.; Hannon, J. B.; Vogel, E. M.; Colombo, L.; Ruoff, R. S. Large-Area Graphene Single Crystals Grown by Low-Pressure Chemical Vapor Deposition of Methane on Copper. *J. Am. Chem. Soc.* **2011**, *133*, 2816–2819.
- (4) Wang, H.; Wang, G.; Bao, P.; Yang, S.; Zhu, W.; Xie, X.; Zhang, W. J. Controllable Synthesis of Submillimeter Single-Crystal Monolayer Graphene Domains on Copper Foils by Suppressing Nucleation. *J. Am. Chem. Soc.* **2012**, *134*, 3627–3630.
- (5) Fan, L.; Li, Z.; Li, X.; Wang, K.; Zhong, M.; Wei, J.; Wu, D.; Zhu, H. Controllable Growth of Shaped Graphene Domains by Atmospheric Pressure Chemical Vapour Deposition. *Nanoscale* **2011**, *3*, 4946–4950.
- (6) Liu, L.; Zhou, H.; Cheng, R.; Yu, W. J.; Liu, Y.; Chen, Y.; Shaw, J.; Zhong, X.; Huang, Y.; Duan, X. High-Yield Chemical Vapor Deposition Growth of High-Quality Large-area AB-Stacked Bilayer Graphene. *ACS Nano* **2012**, *6*, 8241–8249.
- (7) Yu, Q.; Jauregui, L. A.; Wu, W.; Colby, R.; Tian, J.; Su, Z.; Cao, H.; Liu, Z.; Pandey, D.; Wei, D.; Chung, T. F.; Peng, P.; Guisinger, N. P.; Stach, E. A.; Bao, J.; Pei, S.-S.; Chen, Y. P. Control and Characterization of Individual Grains and Grain Boundaries in Graphene Grown by Chemical Vapour Deposition. *Nat. Mater.* **2011**, *10*, 443–449.
- (8) Luo, B.; Chen, B.; Meng, L.; Geng, D.; Liu, H.; Xu, J.; Zhang, Z.; Zhang, H.; Peng, L.; He, L.; Hu, W.; Liu, Y.; Yu, G. Layer-Stacking Growth and Electrical Transport of Hierarchical Graphene Architectures. *Adv. Mater.* **2014**, *26*, 3218–3224.
- (9) Wu, B.; Geng, D.; Xu, Z.; Guo, Y.; Huang, L.; Xue, Y.; Chen, J.; Yu, G.; Liu, Y. Self-Organized Graphene Crystal Patterns. *NPG Asia Mater.* **2013**, *S*, e36.
- (10) Yang, R.; Zhang, L.; Wang, Y.; Shi, Z.; Shi, D.; Gao, H.; Wang, E.; Zhang, G. An Anisotropic Etching Effect in the Graphene Basal Plane. *Adv. Mater.* **2010**, *22*, 4014–4019.
- (11) Geng, D.; Wu, B.; Guo, Y.; Luo, B.; Xue, Y.; Chen, J.; Yu, G.; Liu, Y. Fractal Etching of Graphene. *J. Am. Chem. Soc.* **2013**, *135*, 6431–6434.
- (12) Vlassiouk, I.; Fulvio, P.; Meyer, H.; Lavrik, N.; Dai, S.; Datskos, P.; Smirnov, S. Large Scale Atmospheric Pressure Chemical Vapor Deposition of Graphene. *Carbon* **2013**, *54*, 58–67.
- (13) Booth, T. J.; Pizzocchero, F.; Andersen, H.; Hansen, T. W.; Wagner, J. B.; Jinschek, J. R.; Dunin-Borkowski, R. E.; Hansen, O.; Boggild, P. Discrete Dynamics of Nanoparticle Channelling in Suspended Graphene. *Nano Lett.* **2011**, *11*, 2689–2692.
- (14) Meca, E.; Lowengrub, J.; Kim, H.; Mattevi, C.; Shenoy, V. B. Epitaxial Graphene Growth and Shape Dynamics on Copper: Phase-field Modeling and Experiments. *Nano Lett.* **2013**, *13*, 5692–5697.
- (15) Vlassiouk, I.; Regmi, M.; Fulvio, P.; Dai, S.; Datskos, P.; Eres, G.; Smirnov, S. Role of Hydrogen in Chemical Vapor Deposition Growth of Large Single-Crystal Graphene. *ACS Nano* **2011**, *5*, 6069–6076.
- (16) Zhang, L.; Ni, M.; Liu, D.; Shi, D.; Zhang, G. Competitive Growth and Etching of Epitaxial Graphene. *J. Phys. Chem. C* **2012**, *116*, 26929–26931.
- (17) Wei, D.; Lu, Y.; Han, C.; Niu, T.; Chen, W.; Wee, A. T. Critical Crystal Growth of Graphene on Dielectric Substrates at Low Temperature for Electronic Devices. *Angew. Chem.* **2013**, *125*, 14371–14376.
- (18) Yonhua, T.; Kengchih, L.; Chih-Yi, L.; Chun-Cheng, C.; Yikuan, W. In Controlled Nucleation and Growth of Graphene: Competitive Growth and Etching in Hydrogen Diluted Methane. *Nanotechnology (IEEE-NANO)*; 12th IEEE Conference, August 20–23, 2012; IEEE: New York, 2012; pp 1–4.
- (19) Zhang, Y.; Zhang, L.; Zhang, P.; Ge, M.; Li, Z.; Zhou, C. Vapor Trapping Growth of Single-Crystalline Graphene Flowers: Synthesis, Morphology, and Electronic Properties. *Nano Lett.* **2012**, *12*, 2810–2816.
- (20) Zhang, X.; Ning, J.; Li, X.; Wang, B.; Hao, L.; Liang, M.; Jin, M.; Zhi, L. Hydrogen-Induced Effects on the CVD Growth of High-Quality Graphene Structures. *Nanoscale* **2013**, *5*, 8363–8366.
- (21) Ma, T.; Ren, W.; Zhang, X.; Liu, Z.; Gao, Y.; Yin, L. C.; Ma, X. L.; Ding, F.; Cheng, H. M. Edge-Controlled Growth and Kinetics of Single-Crystal Graphene Domains by Chemical Vapor Deposition. *Proc. Natl. Acad. Sci. U. S. A.* **2013**, *110*, 20386–20391.
- (22) Ma, T.; Ren, W.; Liu, Z.; Huang, L.; Ma, L.-P.; Ma, X.; Zhang, Z.; Peng, L.-M.; Cheng, H.-M. Repeated Growth–Etching–Regrowth for Large-area Defect-Free Single-Crystal Graphene by Chemical Vapor Deposition. *ACS Nano* **2014**, *8*, 12806–12813.
- (23) Zhang, Y.; Li, Z.; Kim, P.; Zhang, L.; Zhou, C. Anisotropic Hydrogen Etching of Chemical Vapor Deposited Graphene. *ACS Nano* **2012**, *6*, 126–132.
- (24) Nie, S.; Wofford, J. M.; Bartelt, N. C.; Dubon, O. D.; McCarty, K. F. Origin of the Mosaicity in Graphene Grown on Cu (111). *Phys. Rev. B: Condens. Matter Mater. Phys.* **2011**, *84*, 155425.
- (25) Vlassiouk, I.; Smirnov, S.; Regmi, M.; Surwade, S. P.; Srivastava, N.; Feenstra, R.; Eres, G.; Parish, C.; Lavrik, N.; Datskos, P.; Dai, S.; Fulvio, P. Graphene Nucleation Density on Copper: Fundamental Role of Background Pressure. *J. Phys. Chem. C* **2013**, *117*, 18919–18926.
- (26) Ci, L.; Xu, Z.; Wang, L.; Gao, W.; Ding, F.; Kelly, K.; Yakobson, B.; Ajayan, P. Controlled Nanocutting of Graphene. *Nano Res.* **2008**, *1*, 116–122.

## Supporting information

### Etching-Controlled Growth of Graphene by Chemical Vapor Deposition

Birong Luo,<sup>†</sup> Enlai Gao,<sup>‡</sup> Dechao Geng,<sup>†</sup> Huaping Wang,<sup>†</sup> Zhiping Xu,<sup>\*,‡</sup> and Gui Yu<sup>\*,†,§</sup>

<sup>†</sup>Beijing National Laboratory for Molecular Sciences, Institute of Chemistry, Chinese Academy of Sciences, Beijing 100190, P. R. China

<sup>‡</sup>Applied Mechanics Laboratory, Department of Engineering Mechanics and Center for Nano and Micro Mechanics, Tsinghua University, Beijing 100084, P. R. China

<sup>§</sup>University of Chinese Academy of Sciences, Beijing 100049, China

E-mail: yugui@iccas.ac.cn; xuzp@tsinghua.edu.cn

#### 1 Experiment parameters

Table S1. The experiment parameters of the etching-controlled growth of graphene on Cu surface by low pressure chemical vapor deposition.

Experiment number (#)	The flow rate ratio of CH <sub>4</sub> to H <sub>2</sub> (sccm)	Growth pressure (Pa)	Growth temperature (°C)	Growth time (min)
1	0.5:15	60	1020	30
2	0.5:20	85		
3	0.5:25	120		
4	0.5:30	160		
5	0.5:35	190		
6	05:40	240		
7	0.5:45	310		
8	0.5:50	410		

## 2 Supplementary SEM and optical microscope characterizations

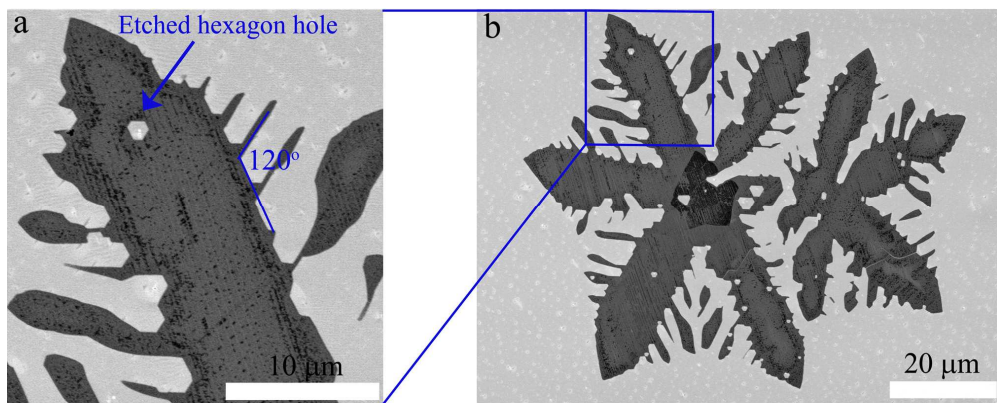


Figure S1. (a) Magnified SEM image taken from a lobe of (b) graphene with etching-controlled growth using a mixture of 0.5 sccm CH<sub>4</sub> and 30 sccm H<sub>2</sub> by low pressure CVD.

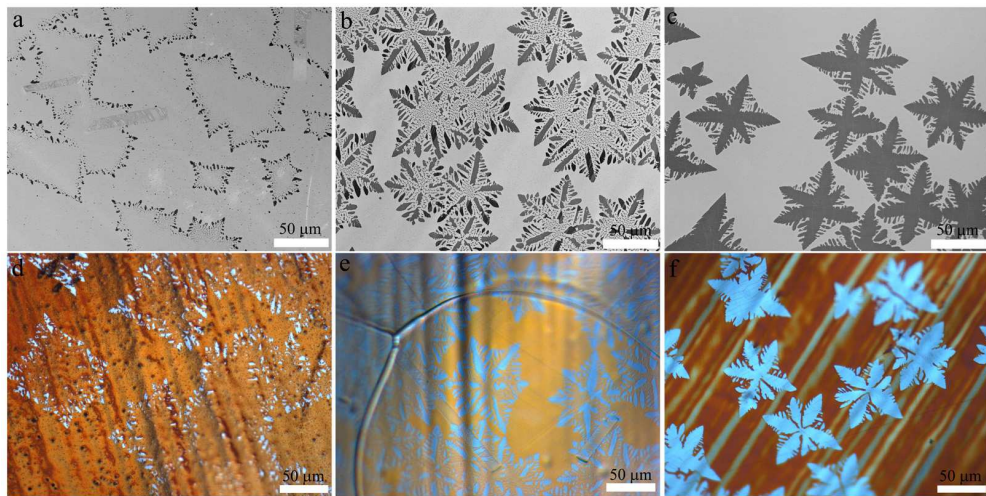


Figure S2. (a-c) SEM images and corresponding (d-f) optical images of graphene with etching-controlled growth using different H<sub>2</sub> flow rate (15, 25, 30 sccm) and 0.5 sccm CH<sub>4</sub>.

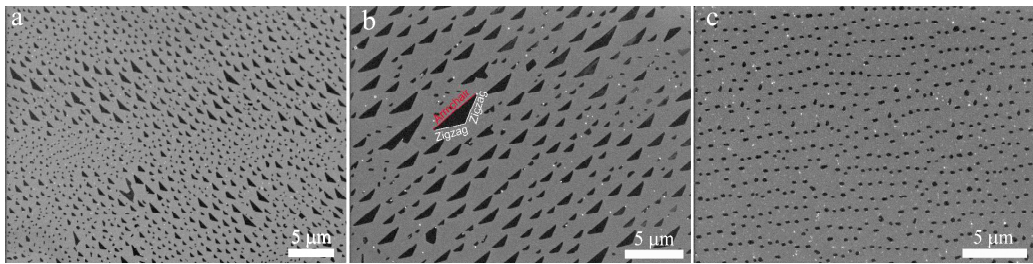


Figure S3. SEM images of graphene debris formed during the etching-controlled growth of graphene using a mixture of 0.5 sccm CH<sub>4</sub> and 20 sccm H<sub>2</sub> by low pressure CVD.

#### 4 Details of phase-field theory and the simulations

In phase-field models [1-3], one order parameter is introduced to characterize the phase of material, which varies smoothly between multiple phases with a diffused interface of finite width. In our simulations to simulate the growth and etching patterns of graphene, the phase-field model consists of an order parameter  $\psi$  and a concentration field  $u$  for the carbon species. The order parameter  $\psi$  equals -1 for the graphene-absent substrate and 1 for the graphene layer. In addition, it is generally agreed that the CVD growth process of graphene on copper follows nucleation-growth model, which begins with an influx of precursors onto the copper surface. This leads to a local supersaturation of active carbon species and triggers the nucleation of graphene domains. The growth of these budding nuclei depletes the carbon concentration within their vicinity, leading further expansion growth of graphene. So, based on this view, the dynamics of the growth process are highly influenced by the flux rate of precursors ( $F$ ) onto the Cu surface and further the concentration of the carbon species ( $u$ ). Here our phase-field simulation also includes these two critical parameters. With carbon species deposited onto the substrate with flux  $F$ , the concentration field is  $u(x, y)$ , and the equilibrium concentration of the carbon species on the surface is  $u_{eq}$ .

The relation between  $u$  and  $u_{\text{eq}}$  determines whether the growth and etching process is dominating. The free energy functional  $G(\psi, u)$  is constructed based on that given by Karma and Plapp [1,3], which can be expressed as

$$G = \int \frac{1}{2} \varepsilon^2 |\nabla \psi|^2 + \frac{1}{\pi} \cos[\pi(\psi - \psi_0)] - \varphi(u - u_{\text{eq}}) \{\psi + \frac{1}{\pi} \sin[\pi(\psi - \psi_0)]\} \quad (1)$$

The growth equations for  $\psi$  and  $u$  can be written as,

$$\begin{aligned} \tau_\psi \frac{\partial \psi}{\partial t} &= -\frac{\partial G}{\partial \psi} \\ &= -\frac{\partial}{\partial x} (\varepsilon \varepsilon' \frac{\partial \psi}{\partial y}) + \frac{\partial}{\partial y} (\varepsilon \varepsilon' \frac{\partial \psi}{\partial x}) + \varepsilon^2 \nabla^2 \psi + \nabla(\varepsilon^2) \cdot \nabla \psi \\ &\quad + \sin[\pi(\psi - \psi_0)] + \varphi(u - u_{\text{eq}}) \{1 + \cos[\pi(\psi - \psi_0)]\} \end{aligned} \quad (2)$$

$$\tau_\psi \frac{\partial u}{\partial t} = D \nabla^2 u + \frac{(1-\psi)}{2} (F - \frac{u}{\tau_s}) - \frac{1}{2} \frac{\partial \psi}{\partial t} \quad (3)$$

Here  $\varepsilon$  is a small parameter which determines the thickness of the interface. The anisotropy of the graphene edge energy is included in terms  $\varepsilon = \varepsilon_0[1+\delta \cos(n\theta)]$  and  $\varepsilon' = -\varepsilon_0 \delta n \sin(n\theta)$ , where  $\varepsilon_0$  is the mean value of  $\varepsilon$ ,  $\delta$  is the strength of the anisotropy and  $n$  corresponds to the symmetry ( $n = 6$  for six-fold anisotropy in this work). The characteristic time of attachment of the carbon species is  $\tau_\psi$ , the mean life time of the species on the surface is  $\tau_s$  with  $\tau_\psi \ll \tau_s$ .  $F$  is the flux of the carbon species arriving at the surface,  $\varphi$  is a dimensionless coupling constant and  $D$  is the diffusion coefficient of the carbon species. The minima of the free energy  $G$  is at  $\psi - \psi_0 = 2m+1$ , where  $m$  is an integer that is independent of  $u$ . The growth morphology of graphene is controlled by the competition among a few parameters, such as the flux  $F$ , equilibrium concentration of the carbon species  $u_{\text{eq}}$ , and the diffusion coefficient  $D$  ( $D$

is a constant in this work), but its symmetry is controlled by the graphene edge energy, that is, six-fold anisotropy.

The equations are discretized in both space and time, with a  $512 \times 512$  spatial mesh, and solved using the finite difference method (in the nine-point finite difference scheme) with periodic boundary conditions applied in the two in-plane directions. We start with a circular nucleus of radius 10 and initial concentration  $3u_{\text{eq}}$ . Simulations are carried at different values of  $F$  and  $u_{\text{eq}}$ , and the results are shown as Figure 6 and S4. The parameters used to generate the results here are  $D = 60$ ,  $\delta = 0.04$ ,  $\tau_\psi = 1.0$ . It should be noted that, further consider the etching process starting from the nucleation point for growth, we initialized a hole in the center of grown graphene pattern and adjust  $u_{\text{eq}}$  to let  $u - u_{\text{eq}}$  in Eq. 2 be negative (Figure. 6a), which reflects the fact that the catalyst there could lower the reaction barrier and facilitate the etching process from inside out.

## Reference

- [1] Karma A., M. Plapp, M. *Phys. Rev. Lett.* **1998**, *81*, 4444-.
- [2] Hao Y., *Science* **342**, 720 (2013).
- [3] Kobayashi, R., *Physica D: Nonlinear Phenomena* **1993**, *63*, 410.

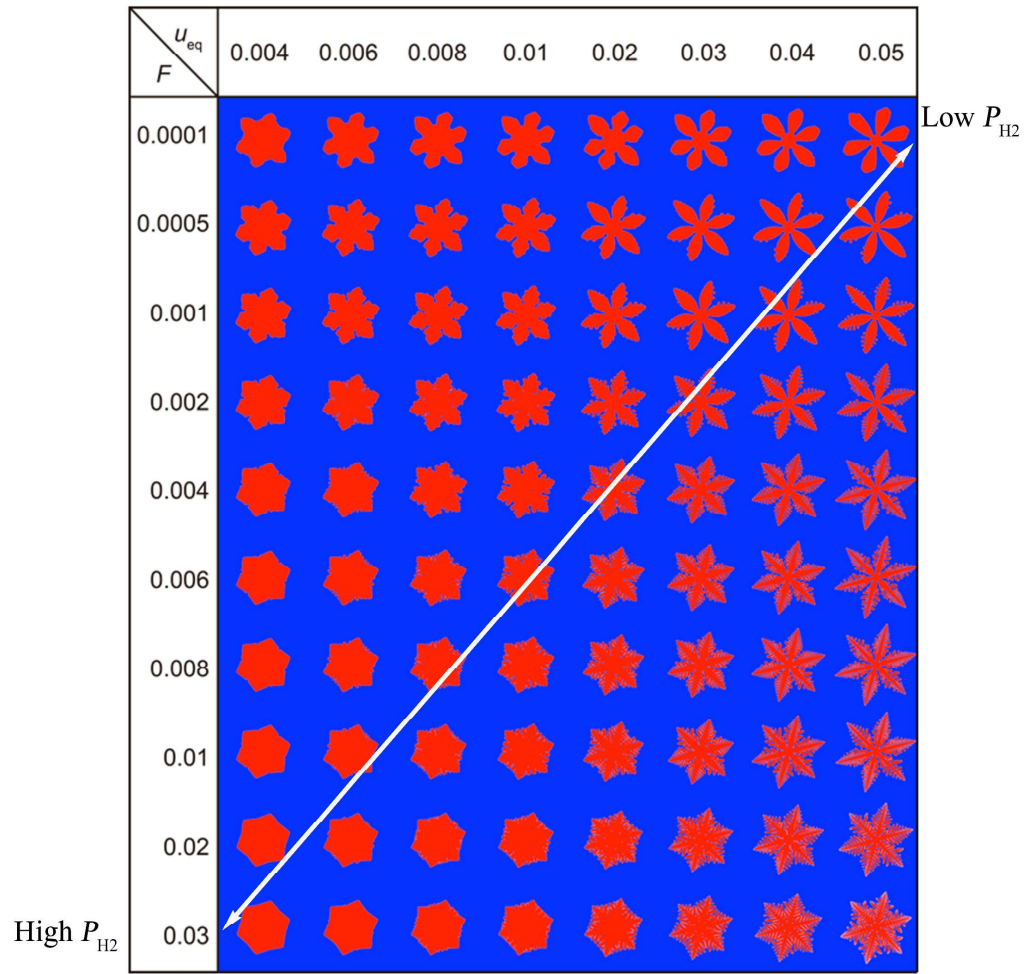


Figure S4. Phase field simulation results for the growth patterns at different values of  $F$  and  $u_{\text{eq}}$ .

## 5 Growth of conventional graphene

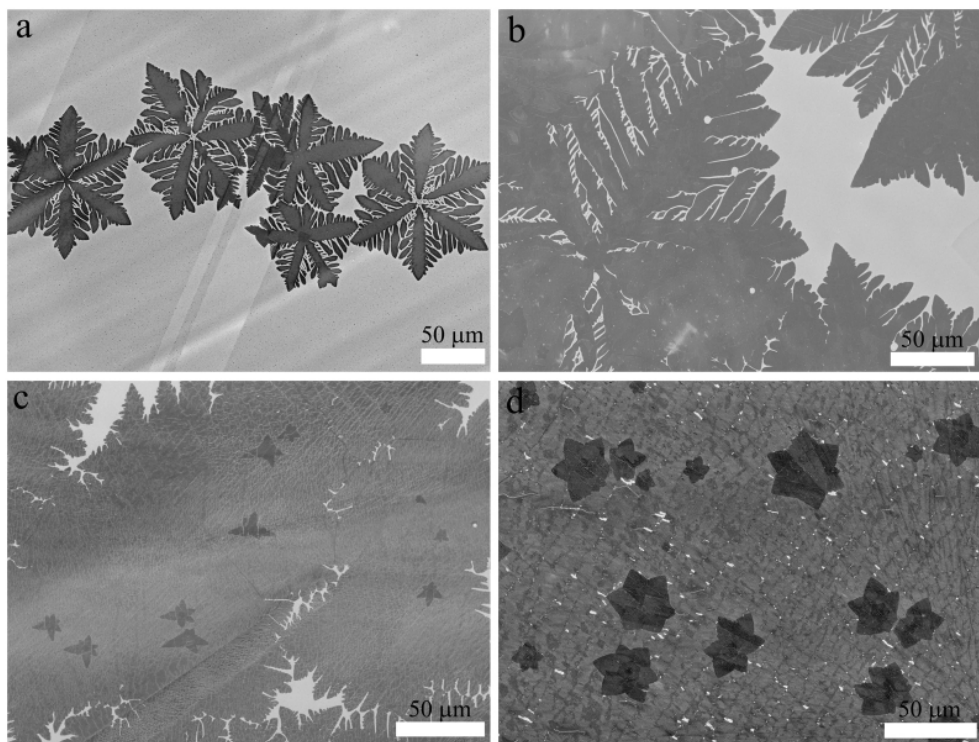


Figure S5. (a-c) Evolution of etching-controlled growth of graphene recorded as a function of  $\text{CH}_4$  flow rate from 0.5, 1.5, 3, to 5 sccm under the fixed  $\text{H}_2$  flow rate of 25 sccm at 1020 °C.